SEARCH FOR PRODUCTION OF STRANGELETS IN QUARK MATTER USING PARTICLE CORRELATIONS

S. Soff, D. Ardouin‡, C. Spieles, S. A. Bass, H. Stöcker

Institut für Theoretische Physik, J. W. Goethe-Universität,
Postfach 11 19 32, D-60054 Frankfurt am Main, Germany; §

D. Gourio, S. Schramm

GSI Darmstadt, Postfach 11 05 52, D-64220 Darmstadt, Germany;

C. Greiner

Institut für Theoretische Physik, J. Liebig-Universität,
Heinrich-Buff-Ring 16, D-35392 Gießen, Germany;

R. Lednicky

Institute of Physics of the Academy of Sciences of the Czech Republic,
Na Slovance 2, 18040 Prague 8, Czech Republic;

V. L. Lyuboshitz

JINR Dubna, PO Box 79, Moscow, Russia;

J.-P. Coffin, C. Kuhn

CRN Strasbourg, Université L. Pasteur, Strasbourg, France.

Abstract. We present a new technique for observing the strangelet production in quark matter based on unlike particle correlations. A simulation is presented with a two-phase thermodynamical model.

‡ on leave from University of Nantes, U.M.R. Subatech

§ supported by GSI, BMBF, DFG and Buchmann Fellowship

1. Motivation

It has been speculated that the observation of strange quark matter droplets might be an unambiguous way to follow up the transient existence of a quark gluon plasma (QGP) expected to be created in ultrarelativistic heavy ion collisions. Due to the Pauli principle, replacing several up and down quarks (u,d) by strange quarks (s), will lower the Fermi energy and the mass of strangelets consisting of multi-quark droplets. Their mass can thus become smaller than the mass of a corresponding ordinary nucleus (with the same baryon number B) and may then correspond to a stable state [1, 2]. The mass per baryon of a strangelet may also be intermediate between the Λ mass and the nucleon mass thus producing a metastable state which then cannot decay into Λ's [3]. Both predictions are found in the MIT bag model, when its energy density constant $B^{1/4}$ is varied (B is the crucial parameter). Large $B^{1/4}$ values ($> 180\,\mathrm{MeV}$) lead to large quark matter droplet masses and therefore to instability versus strong decays. Strangelets are found to be stable for $B^{1/4} \leq 150\,\mathrm{MeV}$ and metastable for intermediate $B^{1/4}$ values [4, 5].

Several experiments are carried out at the Brookhaven AGS (E864, E878) and the CERN SPS (NA52), which look for strangelet production (small Z/A ratios) [6, 7, 8]. Here we present a novel method, which can allow for the measurement of the transient strange quark matter state, even if it decays on strong interaction time scales. The method is based on unequal particle correlations; they are sensitive to the time dependent charge and space-time expansion of the system.

2. The Two-Phase Thermodynamical Model

The dynamical evolution of the mixed phase consisting of a quark gluon plasma and hadronic gas can be described in a two-phase model which takes into account equilibrium as well as non-equilibrium features [9, 10].

Two main assumptions are made :

1. The QGP is surrounded by a layer of hadron gas and equilibrium is maintained during the evolution.

The Gibbs equilibrium conditions write:

$$\begin{aligned} P_{\mathrm{qgp}} &= P_{\mathrm{hadr}} \\ T_{\mathrm{qgp}} &= T_{\mathrm{hadr}} \\ \mu_{\mathrm{q,qgp}} &= \mu_{\mathrm{q,hadr}} \\ \mu_{\mathrm{s,qgp}} &= \mu_{\mathrm{s,hadr}}\,. \end{aligned} \tag{1}$$

2. Non-equilibrium evaporation is incorporated by a time dependent emission of hadrons from the surface of the hadronic fireball. The rate of frozen-out hadrons is assumed to

be governed by the actual hadronic time dependent densities with an universal effective relative rate Γ [9]. The volume change ($\mathrm{d}V$) during the evolution of the plasma is determined by the thermodynamical energy according to:

$$\mathrm{d}E = T\,\mathrm{d}S - p\,\mathrm{d}V + \sum_i \mu_i\,\mathrm{d}N_i\,. \tag{2}$$

In this model the volume increase of the expanding system competes with the volume decrease caused by freeze-out emission. Within this model, it is possible to follow the evolution of mass, entropy and strangeness fraction of the system. From this, relative yields of particles can be extracted which compare reasonably well with experimental data [11].

Fig.1 shows the predicted evolution of the quark chemical potential μ_q. It decreases from $\mu_\mathrm{q} \approx 115\,\mathrm{MeV}$ to $\mu_q^\mathrm{final} \approx 15\,\mathrm{MeV}$ during the hadronization process. Conversely, the s quark chemical potential μ_s increases from $\mu_\mathrm{s} = 0\,\mathrm{MeV}$ to several tens of MeV. Consequently, the strangeness fraction $f_s = (N_s - N_{\bar{s}})/A_\mathrm{tot}$ increases. This leads to a strange multi-quark object if the bag constant $B^{1/4}$ is sufficiently small to allow for cooling of the system (see fig.2).

An important new aspect of these calculations is the fact that the system necessarily leaves the usual $\mu_\mathrm{q} - T$ plane of the phase diagram. It enters quickly into the strangeness sector. Two important features emerge from these calculations [12] (see fig.3 as an example):
1) Strange and anti-strange quarks, produced in equal amount in the hot plasma, do not hadronize at the same time (in a baryon rich system). This so-called "distillation process" [12] results in the formation of stable or metastable blobs of strange matter in the case of low bag model constants. (In this case, a cooling of the system is predicted.) The evaporation from the surface of the hadron gas which is rich of anti-strangeness carries away K^+ etc. thus charging up the remaining mixed system with net positive strangeness.
2) The large f_s ($\approx 1.5 - 2$) attained imply negative charge-to-mass ratios ($Z/A = -0.1$ for stable, $Z/A = -0.45$ for metastable droplets).

In the present work, these time separation and negative charge values characterize the transient existence of the plasma. They can be used to search for the distillation process by correlations of unlike particles.

3. Influence of Coulomb Interactions on Particle Interferometry

In the case of charged particles (like K^+, K^-), their Coulomb interaction modifies the plane and outgoing scattered waves and the two-particle amplitude takes the form:

$$\psi^+_{-\vec{k}} = \mathrm{e}^{i\delta}\sqrt{A(\eta)}\left[\mathrm{e}^{-i\vec{k}\vec{r}}F(-i\eta, 1, i\rho) + \Phi^c_k(r)\right], \tag{3}$$

where δ is the Coulomb s–wave phase shift, $F(-i\eta, 1, i\xi)$ is the confluent hypergeometric function, $\rho = \vec{kr} + kr$, $\eta = (ka)^{-1}$, $|a|$ is the Bohr radius of the two–particle system, $\Phi_k^c(r)$ is the scattered wave, and

$$A(\eta) = 2\pi\eta[\exp(2\pi\eta) - 1]^{-1} \tag{4}$$

is the well known Coulomb factor. The $A(\eta)$ factor differs from unity mainly for $|2\pi\eta|^{-1} < 1$ which means $k < 12$ MeV/c in the case of the K^+K^- system ($a = -110$ fm). At high energies the two-body Coulomb effect is often treated through a size-independent correction factor $A(\eta)$ to the usual quantum statistical correlations (i.e., it is assumed that $r/|a| \ll 1$ so that $F(-i\eta, 1, i\rho) \approx 1$). It is thus not used to study the space-time evolution of the system. Contrary, at low energies this effect becomes the main tool for the study of this evolution due to large transit times. In addition, the charged source itself can also affect the above two-particle correlation pattern due to the long range interaction (e.g. accelerating K^+ and deaccelerating K^- for $Z > 0$). This effect is much more clearly visible in the single particle spectra, while it nearly cancels out (by taking the denominator) in the correlation function.

Experimental evidence and detailed analysis of such Coulomb two- and three-body effects on two unlike particle correlation functions can be found in [13]. The three-body effect itself was observed experimentally more than ten years ago [14] in intermediate energy heavy ion collisions and quantitatively analyzed in reactions producing light particles or unstable fragments (Li*, B*) and short-lived resonant states. If their decay occurs into two different particles (with different charge/mass ratios) within the Coulomb field of the residual nuclear system (target/projectile fragments), this field can substantially distort their correlation function. Thus a complete three-body calculation is required to account for the effect of final state interactions. One way to look at this width/lifetime effect is to compare correlation functions measured for different relative velocities [14, 15]. One then observes a shift of the resonance peak which reflects the different Z/A values of the coincident particles which suffer the Coulomb accelerations. This effect has been later used to explain a variety of two particle correlation patterns in the intermediate energy domain [16]. In the adiabatic limit, it has also been studied within a detailed and full three-body quantum approach [17, 18]. This effect is found to decrease for particles emitted at large relative space-time intervals or with large momenta with respect to the source. It is increasing with increasing source charge and also with increasing charges and masses of the particles.

4. Access to Time Sequence of Emission using Unlike-Particle Correlations

In addition to the known directional dependence of the correlations of two identical particles, it has been shown (at low energy heavy ion collisions) that the final state

interactions between non-identical particles can provide information about the time-order of emission. Thus, based on classical trajectory calculations, it was proposed to use the velocity difference spectrum between two different charged particles and examine its dependence on particle energy in conjunction with the corresponding relative momentum correlation function [19]. Independently, in the quantum approach [17, 20] it was shown that the anisotropy of the space-time distribution is reflected in the directional dependence of unlike-particle correlations and can be directly used to measure the delays in the emission of particles of different types.

With the assumption of a sufficiently small density in momentum space, the correlation is only due to the mutual final state interaction; the two-particle amplitude, in the absence of the Coulomb interaction, takes the form [21]:

$$\psi^{+}_{-\vec{k}} = \mathrm{e}^{-i\vec{k}\vec{r}} + \Phi_k(r)\,, \tag{5}$$

where $\vec{k} = \vec{q}/2$ and $\vec{r}$ are the relative momentum and spatial coordinates of the two particles in their cms system, $\Phi_k(r)$ is the scattered wave. The correlation function for two non-identical particles is

$$1 + R(p_1, p_2) = 1 + \langle |\Phi_k(r)|^2 + 2\,\mathrm{Re}\,\Phi_k(r)\cos(\vec{k}\,\vec{r}) - 2\,\mathrm{Im}\,\Phi_k(r)\sin(\vec{k}\,\vec{r})\rangle\,. \tag{6}$$

The directional dependence in the correlation function [20] is contained in the odd term, $\mathrm{Im}\,\Phi_k(r)\sin(\vec{k}\,\vec{r})$. In the limit of large relative emission times $t = t_1 - t_2$, $v|t| \gg r$, the vector $\vec{r}$ is only slightly modified by averaging over the spatial location of the emission points in the rest frame of the source. So the vector $\vec{r}$ is nearly parallel or antiparallel to the pair velocity $\vec{v}$ depending on the sign of the time difference. The odd part of the correlation function is sensitive to this sign. This mean relative emission time, including its sign can be determined by comparing the correlation functions R^+ and R^- [20]. In these functions the sign of the scalar product $\vec{k}\cdot\vec{v}$ is fixed to be larger or smaller than zero (using their relative angle) respectively. Note that for particles of equal masses the sign of $\vec{k}\cdot\vec{v}$ is almost equal to the sign of the velocity difference $v_1 - v_2$. This means that the interaction of the two particles will be different in the case where the faster particle is emitted earlier as compared to the case of its later emission.

In the case of unlike *charged* particles, additional odd terms in the $\vec{k}\cdot\vec{r}$ product appear due to the confluent hypergeometrical function. This modifies the plane wave and preserves the sensitivity to the time difference even in the case of a weak effect of the strong interaction. It has also been shown [21] that the Coulomb field of the residual nucleus slightly affects this result.

These predictions have been compared to experimental (p,d) correlations measured for the Nb+Pb, Xe+Ti, Xe+Sn collisions studied at GANIL [22, 23, 24, 25]. The ratio $(1 + R^+)/(1 + R^-)$ deviates from unity at low q. This can be attributed to an earlier emission of deuterons rather than protons on the average. Thus, it has

been experimentally demonstrated for the first time that the study of the directional asymmetries in the correlations of non-identical particles provides a unique tool to measure the time-ordering of particle emission. This technique will here be extended to emission time differences between strange, anti-strange and non-strange particles [20]. We study its sensitivity to the time delays related to the production of the transient strange quark matter state.

5. Calculations with an Event Generator

A quantum two-particle final state interaction code [21] is used together with a three-body calculation [17] to simulate the possible influence on K^+K^- correlations caused by

1) different distributions of the K^+ and K^- emission times and

2) by different charge states of the emitting source.

Results are presented for an event generator describing a mid-rapidity source with transverse mass spectra conditions typical for AGS experiments. The source is assumed to be Gaussian in space coordinates and exponential in time. Different sets of time origins are used for the two particles.

Fig.4 shows some simulations with mean emission time differences between K^+ and K^- of -5 to $+10$ fm/c. The figure shows the ratio of the relative momentum correlation functions $(1+R^+)/(1+R^-)$ as obtained with the above selections for values of the scalar product $\vec{k}\cdot\vec{r} > 0$ and < 0, respectively. Clearly, ratios less than one are associated with a scenario where the K^-'s are emitted later on the average.

Fig.5 shows the dependence of the above ratio on the charge of the source. The time difference is fixed to $+10$ fm/c. The upper diagram shows the result of a 2-body calculation. The two lower diagrams correspond to 3-body calculations with source charges $Z = 50$ and $Z = -50$, respectively. We have checked that the neglection of the strong final state interaction only slightly modifies these results. Therefore, most of the effect originates from the Coulomb interaction between the two kaons with an additional slight enhancement (suppression) of this deviation from unity created by a positive (negative) source charge.

6. Calculations with the Two Phase Thermodynamical Model coupled to Final State Interactions

The previous section clearly shows the domain of sensitivity of the K^+K^- correlations to time differences and charge effects. In order to do similar calculations with a more sophisticated particle source, we have described the source evolution using the thermodynamical model presented in section 2. Three sets of parameters have been

chosen:
set 1 & *2* (representing Au+Au at AGS energies):
initial mass $A = 394$, entropy per baryon $S/A = 10$, initial net strangeness $f_s = 0$;
set 1: $B^{1/4} = 160\,\mathrm{MeV}$, strangelets (albeit metastable) are formed.
set 2: $B^{1/4} = 235\,\mathrm{MeV}$, strangelets are not distilled, their thermal formation is also highly suppressed. They are not (meta-)stable.
set 3 (representing S+Au at SPS energies):
bag model constant $B^{1/4} = 235\,\mathrm{MeV}$,
initial mass $A = 100$, entropy per baryon $S/A = 45$, initial net strangeness $f_s = 0$.
Corresponding calculated time evolutions are shown in figs. 6 and 7 for particle yields, initial quark blob masses and charges. In the case of a high bag constant the system heats up slightly. The entropy per baryon in the QGP is larger than in the hadronic phase. This results in a fast hadronization (see the radius and charge time evolutions). K^+ are emitted earlier than K^-. For low bag constants, a cold strangelet emerges in a few tens of fm/c with a radius of $\approx 2.5\,\mathrm{fm}$, a finite net strangeness content and a **negative** charge.

These predicted time dependent yields are used as input for the final state interaction calculations. Fig.8 shows the calculated correlation function ratios $(1 + R^+)/(1 + R^-)$ for K^+K^- pairs. Similar functional dependencies are found as with the simple event generator calculations.

The ratio of the measured correlation functions for $\vec{k} \cdot \vec{v} > 0$ and $\vec{k} \cdot \vec{v} < 0$ shows that the K^- is emitted later in the case of a low bag constant value. The effect is seen as a $30 - 35\%$ dip relative to equal mean time production ($R = 1$). It extends up to $q \approx 30\,\mathrm{MeV/c}$ for the parameters of *set 1*.

A weaker effect (10%) is found, extending up to $q \approx 40\,\mathrm{MeV/c}$ when *set 2* (high bag constant) is used. The effect is nearly gone for the higher initial entropy *set 3*. This may be attributed to freeze-out time distributions of K^+ and K^- which are quite similar as seen in the predicted yields (figs. 3 and 7). The slight difference between the sets 2&3 has to be attributed to the smaller Coulomb influence of the source itself ($A = 100$) in the entropy $S/A = 45$ calculation. Our simulations (see fig.5 and discussion above) support this explanation (including the direction of this effect) as long as an averaged positive charge is present (in agreement with the present model calculation displayed in fig.6).

7. CONCLUSION AND PERSPECTIVES

We have presented a novel method, which can allow for the measurement of the transient strange quark matter state, even if it decays on strong interaction time scales. The method is based on unequal particle correlations. They are sensitive to the time

dependent charge and space-time expansion of the system. The dynamical evolution model for the mixed QGP-hadronic phase has been applied to describe the strangeness distillation process. This predicts a time dependent freeze-out and the occurence of low charge-to-mass ratios. The existence of strangelets can thus be characterized by the correlation approach of unlike particles presented here.

Hydrodynamical calculations including the expansion of the system are currently underway. Also microscopic analysis of this effect, based on the UrQMD-simulations, are presently under study. If combined with the identical particle interferometry (HBT), this technique offers the possibility to study different expansion processes associated with different transverse motion and sizes. Correlations of other particles ($p\Lambda$, $p\pi^-$, etc.) are presently studied.

Acknowledgments

The authors would like to thank B. Erazmus, L. Martin, D. Nouais and C. Roy for useful discussions and for providing their correlation codes. D. A. is pleased to thank the Institut für Theoretische Physik at the University of Frankfurt for their invitation and kind hospitality.

References

[1] A. R. Bodmer, Phys. Rev. **D4**, 1601 (1971).
[2] E. Witten, Phys. Rev. **D30**, 272 (1984).
[3] S. A. Chin and A. K. Kerman, Phys. Rev. Lett. **43**, 1292 (1979).
[4] H. W. Barz, B. L. Friman, J. Knoll, H. Schulz, Nucl. Phys. **A484**, 661 (1988).
[5] C. Greiner, D. H. Rischke, H. Stöcker, P. Koch, Phys. Rev. **D38**, 2797 (1988).
[6] R. Klingenberg (NA52 Collaboration), Proceedings of 12th International Conference on Ultra-Relativistic Nucleus-Nucleus Collisions (Quark Matter 96), Heidelberg (Germany), 1996. Nucl. Phys. **A610**, 306c (1996).
[7] F. S. Rotondo (E864 Collaboration), Proceedings of 12th International Conference on Ultra-Relativistic Nucleus-Nucleus Collisions (Quark Matter 96), Heidelberg (Germany), 1996. Nucl. Phys. **A610**, 297c (1996).
[8] M. J. Bennett (E878 Collaboration), Proceedings of 11th International Conference on Ultra-Relativistic Nucleus-Nucleus Collisions (Quark Matter 95), Monterey (California), 1995. Nucl. Phys. **A590**, 491c (1995).
[9] C. Greiner, H. Stöcker, Phys. Rev. **D44**, 3517 (1991).
[10] C. Spieles, L. Gerland, H. Stöcker, C. Greiner, C. Kuhn, J. P. Coffin, Phys. Rev. Lett. **76**, 1776 (1996).
[11] C. Spieles, H. Stöcker, C. Greiner, submitted to Z. Phys. **C**, e-Print Archive: nucl-th/9704008.
[12] C. Greiner, P. Koch, H. Stöcker, Phys. Rev. Lett. **58**, 1825 (1987).
[13] For a review see e.g.: D. H. Boal, C. K. Gelbke, B. K. Jennings, Rev. Mod. Phy. **62** 553 (1990); J. M. Alexander, A. Elmaani, L. Kowalski, N. N. Ajitanand, C. J. Gelderloos, Phys. Rev. **C48**,

2874 (1993); W. Bauer et al., Ann. Rev. Nucl. Sc. **42**, 77 (1992); D. Ardouin, Int. J. Mod. Phys. **6**, n0 1 (1997).

[14] J. Pochodzalla et al., Phys. Lett. **B161**, 256 (1985); J. Pochodzalla et al., Phys. Lett. **B174**, 36 (1986).

[15] J. Pochodzalla et al., Phys. Rev. **C35**, 1695 (1987).

[16] G. Bertsch, P. Danielewicz, H. Schulz, Eur. Lett. **21**, 817 (1993); B. Erazmus et al., Nucl. Phys. **A583**, 395 (1995); B. Erazmus, L. Martin, R. Lednicky, N. Carjan, Phys. Rev. **C49**, 349 (1994).

[17] R. Lednicky et al., Rapport Interne 94-22 Nantes; submitted to Nucl. Phys. **A**.

[18] L. Martin et al., Nucl. Phys. **A604**, 69 (1996).

[19] C. Gelderloos et al., Nucl. Inst. Meth. **A349**, 618 (1994).

[20] R. Lednicky, V. L. Lyuboshitz, B. Erazmus, D. Nouais, Phys. Lett. **B373**, 30 (1996).

[21] R. Lednicky, V. L. Lyuboshitz, Sov. J. Nucl. Phys. **35**, 30 (1982); R. Lednicky, V. L. Lyuboshitz, Proceedings of the Int. Conf. on Nucl. Interferometry -CORINNE I- (1990) edited by D. Ardouin, World Scientific.

[22] C. Ghisalberti et al., Proceedings of the XXXI Int. Bormio Meeting (1993), and Nucl. Phys. **A583**, 401 (1995).

[23] B. Erazmus, Proceedings of the XXXIV Bormio Meeting (1995).

[24] D. Gourio, PhD Thesis (1996), Nantes (unpublished).

[25] D. Nouais, PhD Thesis (1996), Nantes (unpublished).

Figure captions

Figure 1. Time evolution of the quark and strange chemical potential for parameter *set* 3. Hadronic and quark matter rapidly moving out of the $(\mu_{\rm q}, T)$ plane, entering the strange sector ($f_s \neq 0$). The fit of a static thermal source which yields the same hadron ratios as the dynamical model is also depicted.

Figure 2. Time evolution of baryon number A, strangeness fraction f_s and temperature T for $S/A_{\rm init} = 25$ and $f_s = 0.25$ for a (a) high ($B^{1/4} = 235\,{\rm MeV}$) and (b) low ($B^{1/4} = 145\,{\rm MeV}$) bag constant, respectively.

Figure 3. Yields for π^+, K^+, K^-, p and Λ particles as a function of time for the AGS parameter sets 1&2 (upper figure $B^{1/4} = 160\,{\rm MeV}$, lower figure $B^{1/4} = 235\,{\rm MeV}$).

Figure 4. Simulation of different time origins for K^+ and K^- emission with the event generator. Shown are the ratios $(1 + R^+)/(1 + R^-)$ as explained in the text.

Figure 5. Simulation of the influence of the source charge state on the ratio $(1 + R^+)/(1 + R^-)$ with the event generator (see text).

Figure 6. Radius and charge of the remaining quark matter blob as a function of time t as calculated with the two-phase thermodynamical model.

Figure 7. Particle yields as a function of time t for a bag constant $B^{1/4} = 235\,\mathrm{MeV}$, initial entropy $S/A = 45$, initial baryon number $A_{\mathrm{init}} = 100$, representing an SPS parameter set (set 3 in the text).

Figure 8. Ratios of correlation functions $(1 + R^+)/(1 + R^-)$ for three different parameter sets (see text).

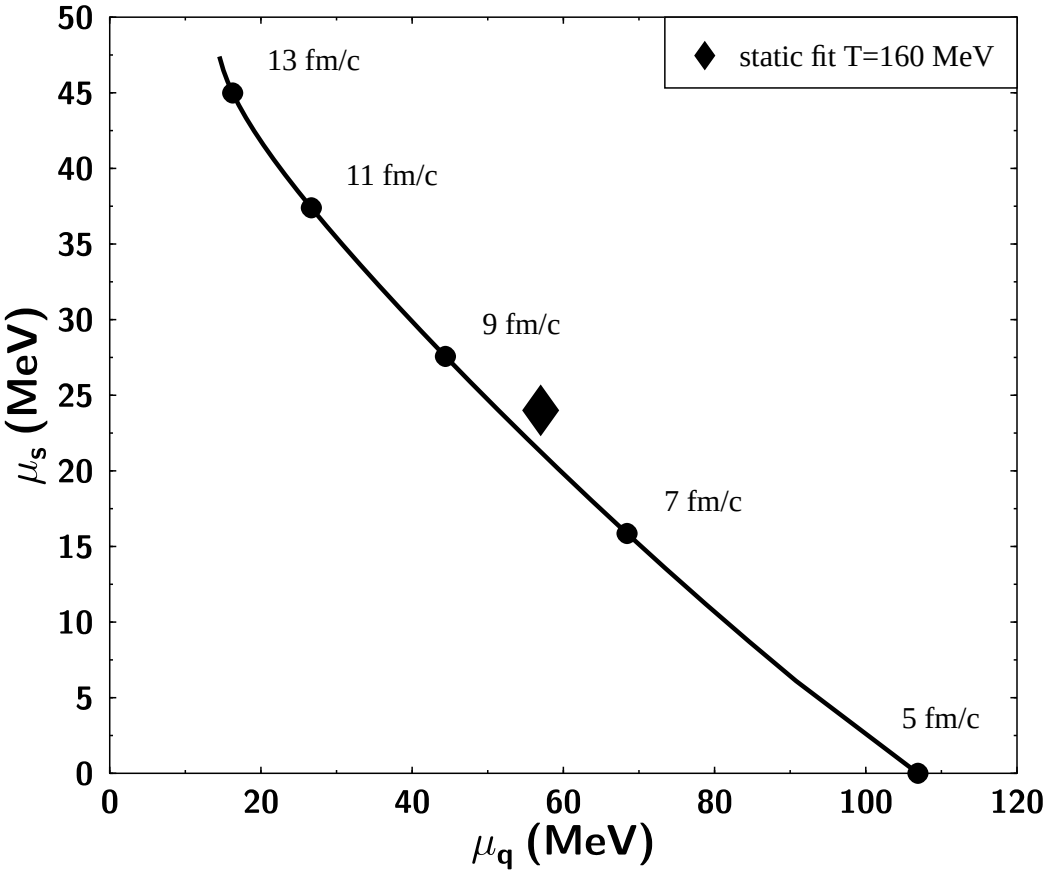
static fit T=160 MeV
13 fm/c
11 fm/c
9 fm/c
7 fm/c
5 fm/c
μ_s (MeV)
μ_q (MeV)
0
5
10
15
20
25
30
35
40
45
50
0
20
40
60
80
100
120

Fig.1

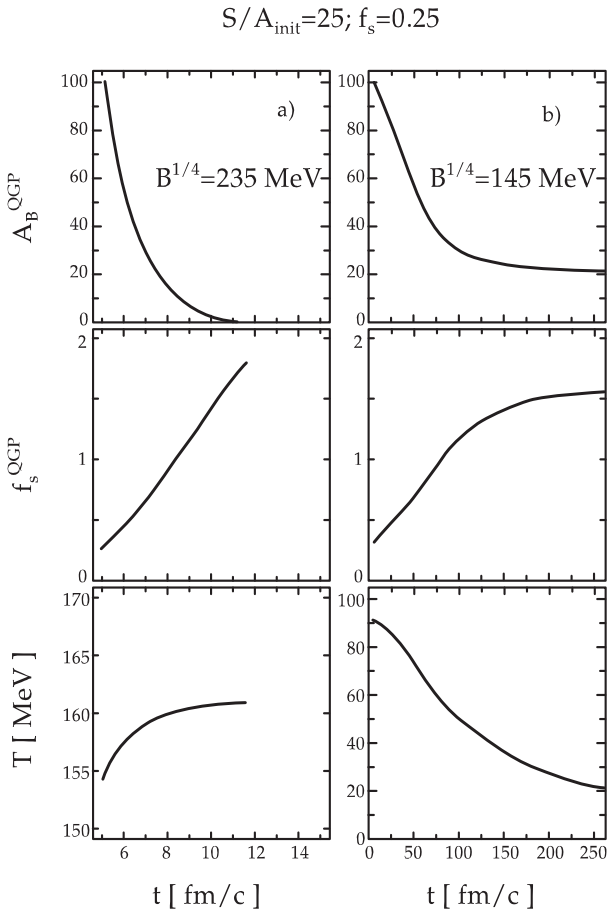
S/A_init=25; f_s=0.25
a)
b)
B^1/4=235 MeV
B^1/4=145 MeV
A_B^QGP
f_s^QGP
T [MeV]
t [fm/c]
t [fm/c]

Fig.2

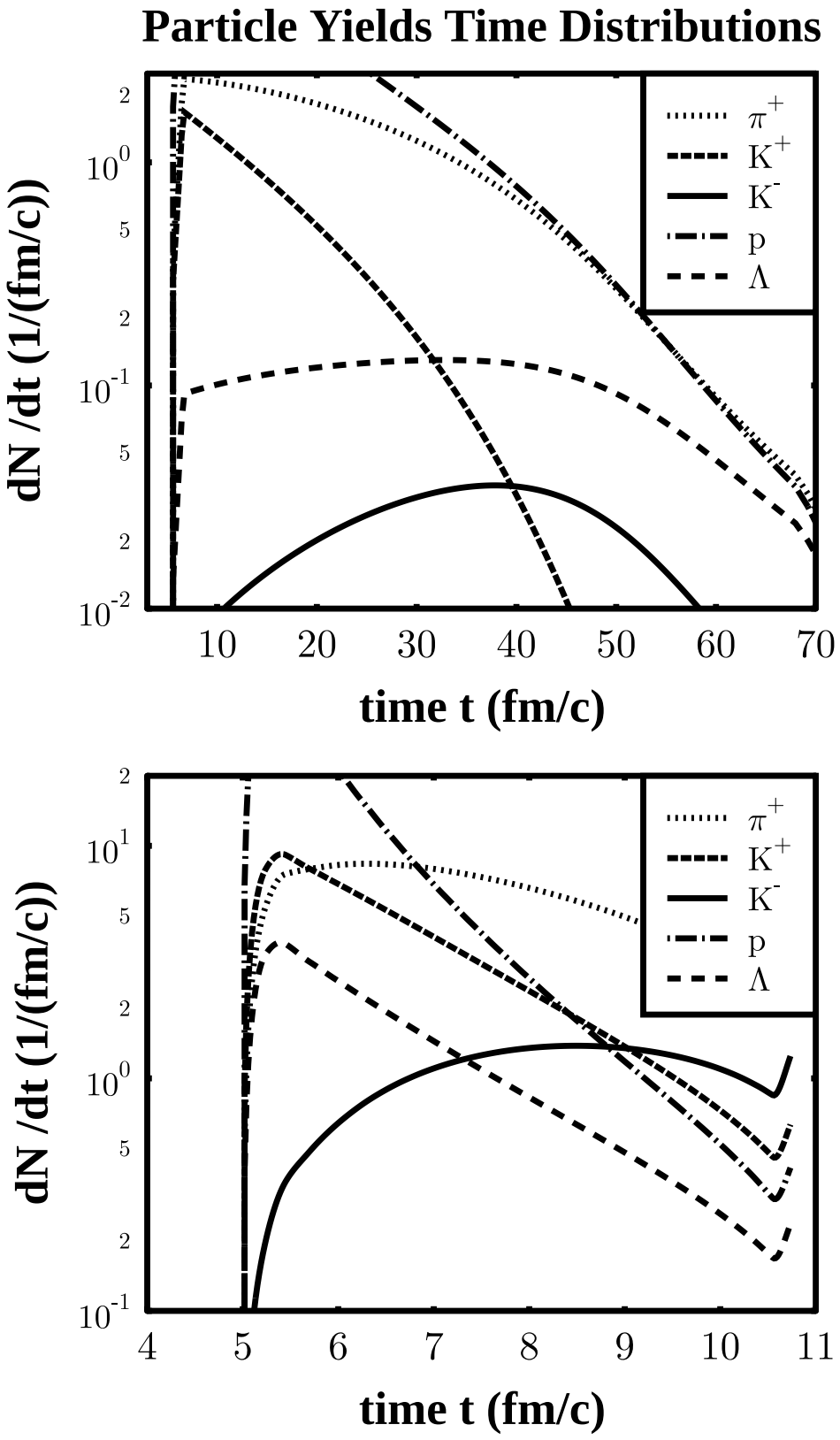
Particle Yields Time Distributions
dN /dt (1/(fm/c))
time t (fm/c)
π+
K+
K-
p
Λ
dN /dt (1/(fm/c))
time t (fm/c)
π+
K+
K-
p
Λ

Fig.3

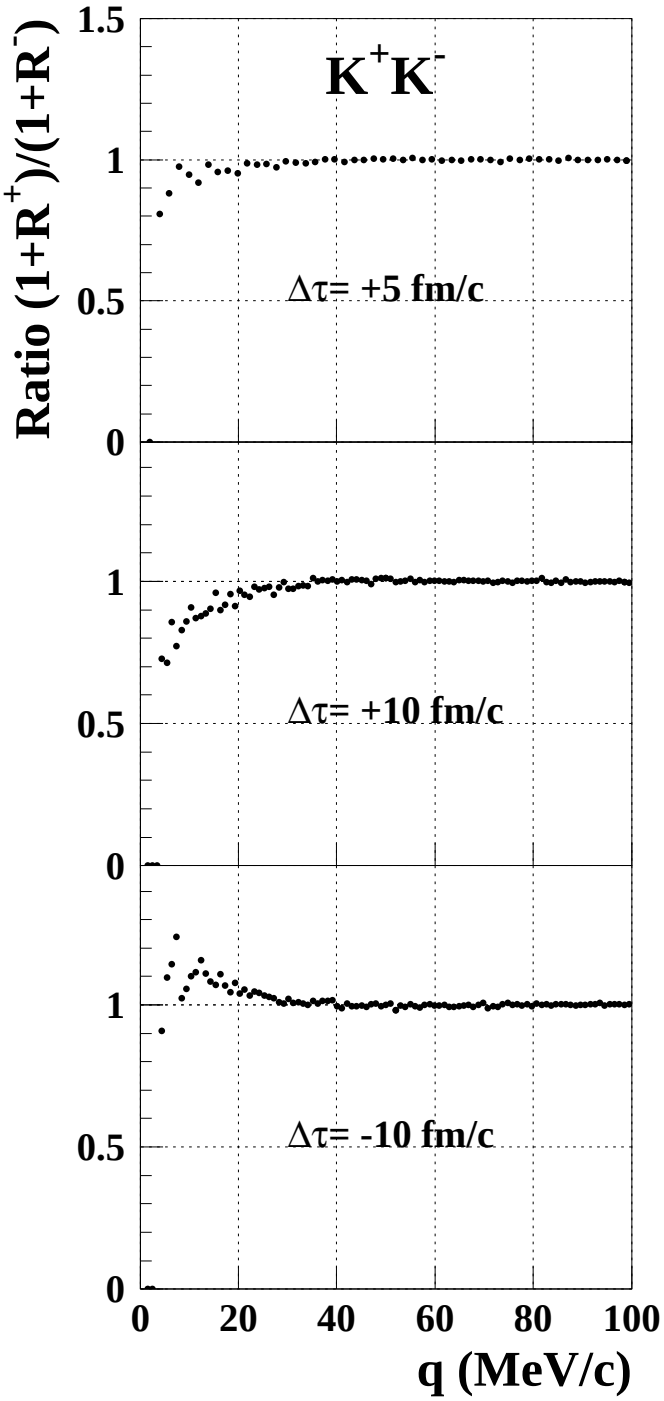
K+K-
Ratio (1+R+)/(1+R-)
Δτ= +5 fm/c
Δτ= +10 fm/c
Δτ= -10 fm/c
q (MeV/c)
0
0.5
1
1.5
0
20
40
60
80
100

Fig.4

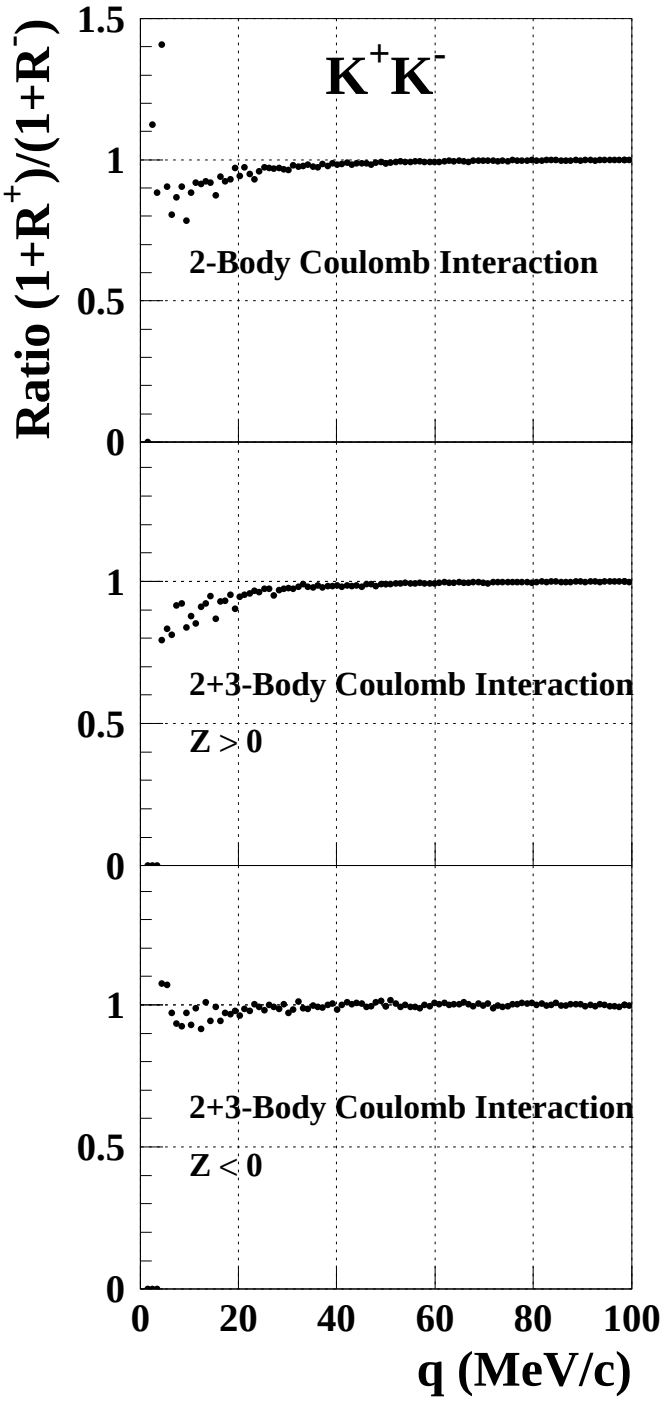
K^+K^-
2-Body Coulomb Interaction
2+3-Body Coulomb Interaction
Z > 0
2+3-Body Coulomb Interaction
Z < 0
Ratio $(1+R^+)/(1+R^-)$
q (MeV/c)
0
20
40
60
80
100
0.5
1
1.5

Fig.5

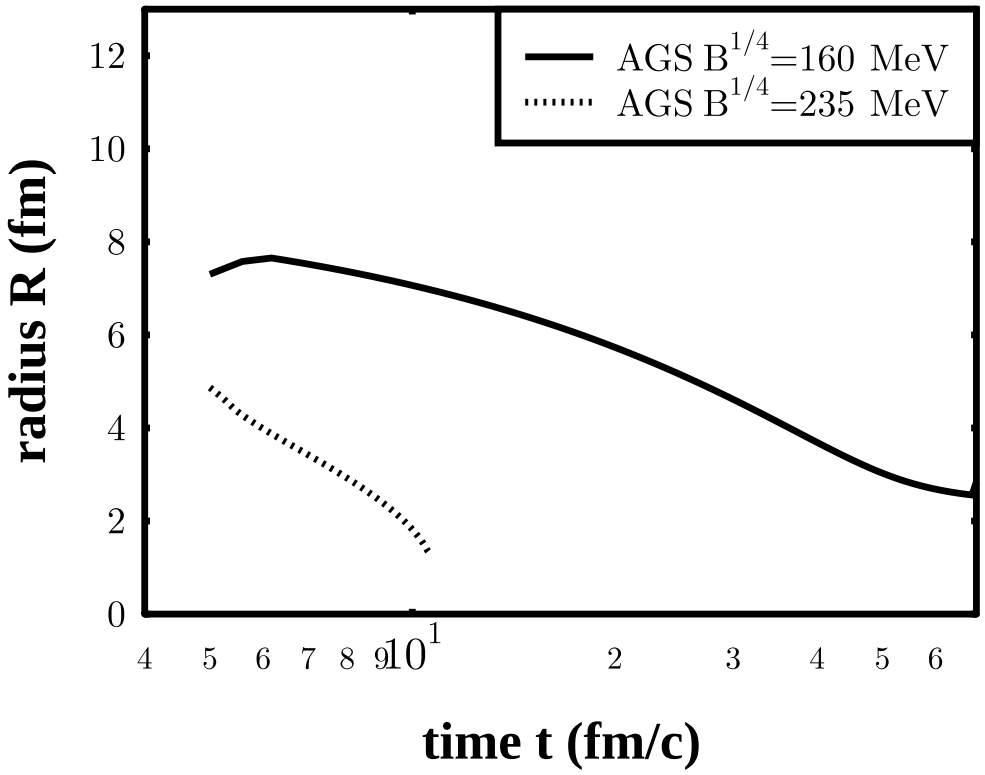
AGS B$^{1/4}$=160 MeV
AGS B$^{1/4}$=235 MeV
radius R (fm)
0
2
4
6
8
10
12
4 5 6 7 8 9 10^1 2 3 4 5 6
time t (fm/c)

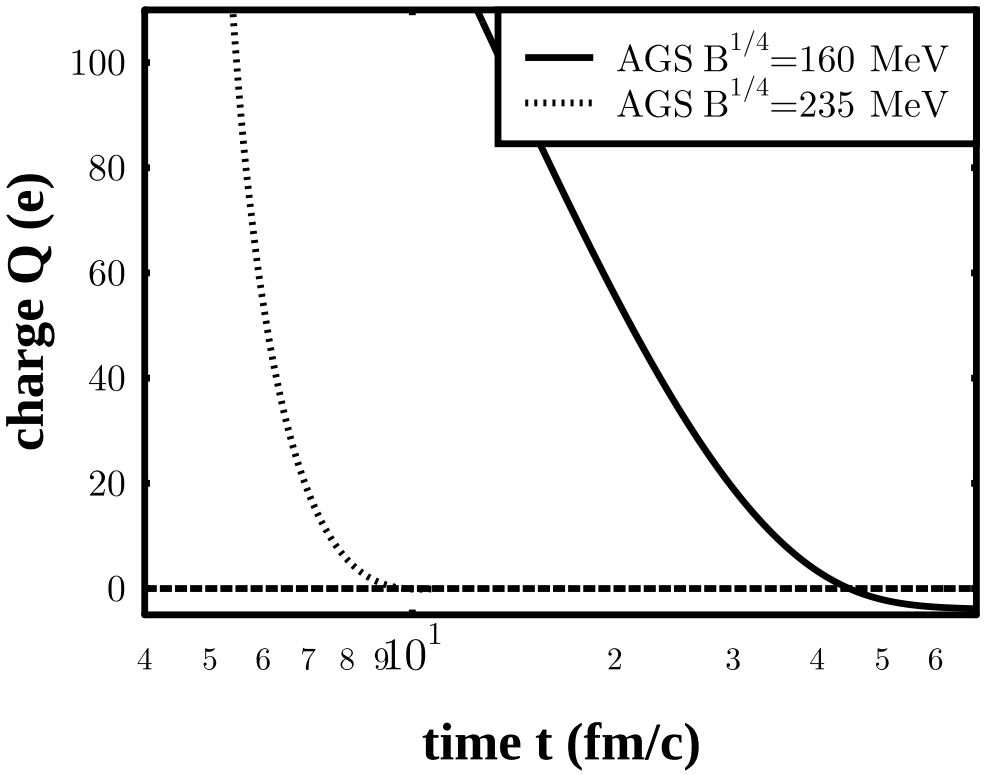
AGS B$^{1/4}$=160 MeV
AGS B$^{1/4}$=235 MeV
charge Q (e)
0
20
40
60
80
100
4 5 6 7 8 9 10^1 2 3 4 5 6
time t (fm/c)

Fig.6

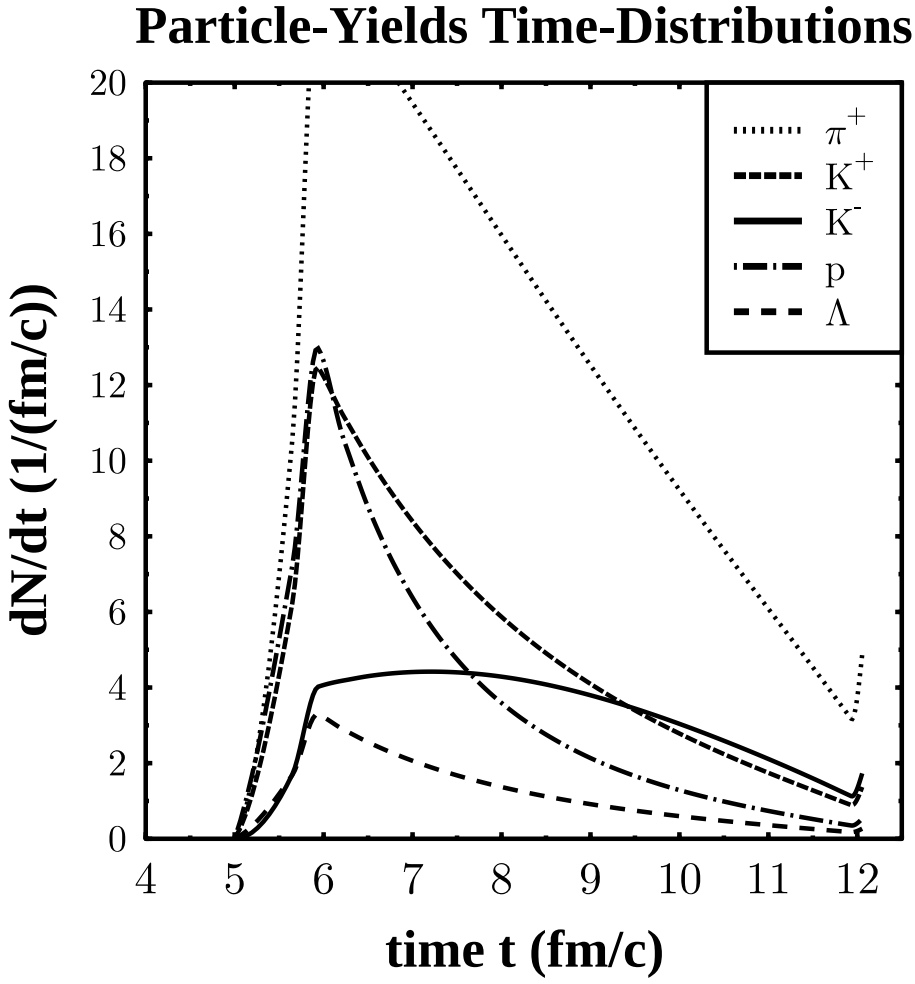
Particle-Yields Time-Distributions
dN/dt (1/(fm/c))
time t (fm/c)
π+
K+
K-
p
Λ
0
2
4
6
8
10
12
14
16
18
20
4
5
6
7
8
9
10
11
12

Fig.7

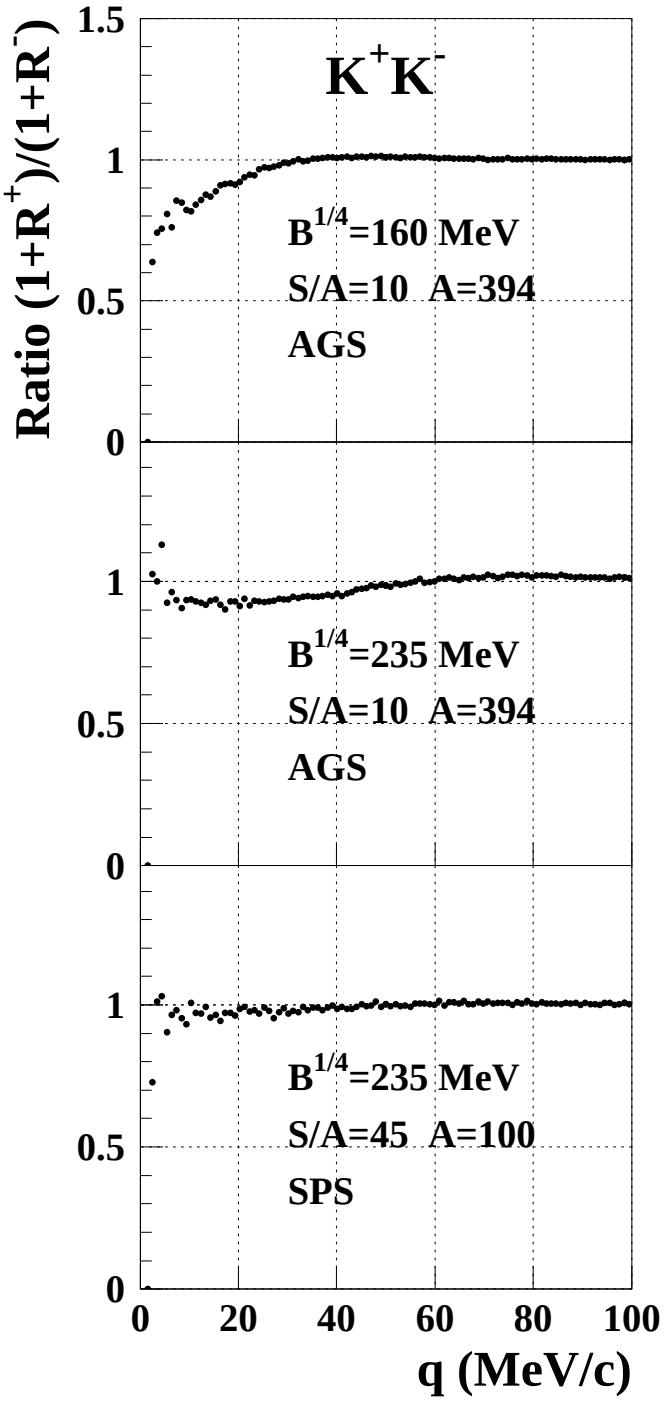
K+K-
Ratio (1+R+)/(1+R-)
B1/4=160 MeV
S/A=10 A=394
AGS
B1/4=235 MeV
S/A=10 A=394
AGS
B1/4=235 MeV
S/A=45 A=100
SPS
q (MeV/c)

Fig.8